

Wavelet Residual Network for Low-Dose CT via Deep Convolutional Framelets

Eunhee Kang, Jaejun Yoo, and Jong Chul Ye*, *Senior Member, IEEE*

Abstract—Model based iterative reconstruction (MBIR) algorithms for low-dose X-ray CT are computationally expensive. To address this problem, we recently proposed the world-first deep convolutional neural network (CNN) for low-dose X-ray CT and won the second place in 2016 AAPM Low-Dose CT Grand Challenge. However, some of the texture were not fully recovered. To cope with this problem, here we propose a deep residual learning approach in directional wavelet domain. The proposed method is motivated by an observation that a deep convolutional neural network can be interpreted as a multilayer convolutional framelets expansion using non-local basis convolved with data-driven local basis. We further extend the idea to derive a deep convolutional framelet expansion by combining global redundant transforms and signal boosting from multiple signal representations. Extensive experimental results confirm that the proposed network has significantly improved performance and preserves the detail texture of the original images.

Index Terms—Wavelet transform, residual network, low-dose CT, convolutional neural network (CNN), convolutional framelets

I. INTRODUCTION

X-RAY computed tomography (CT) is one of the most valuable imaging techniques in clinics. It is used in various ways, including whole-body diagnostic CT, C-arm CT for interventional imaging, dental CT, etc. However, X-ray CT causes potential cancer risks due to radiation exposure. In order to ensure the safety, methods for minimizing X-ray dose were intensively investigated. Conventionally, the reduction in the number of X-ray photons using the tube current modulation is seen as a solution. A drawback of this approach is, however, the low signal-to-noise ratio (SNR) of projections, which induces noise in the reconstructed image.

While the noise of low-dose X-ray CT is often approximated as Gaussian noise, this model is not suitable for streaking noise originating from photon starvation and beam hardening [1]. Various model based iterative reconstruction (MBIR) methods [2], [3], [4] have been investigated to obtain a clear reconstructed image. However, these approaches are usually computationally expensive because of the iterative applications of forward and backward projections.

Recently, deep learning approaches have been actively explored through the use of extensive data and powerful graphical processing units (GPUs). With the new network units such as rectified linear unit (ReLU), max pooling and batch

normalization, deep networks have achieved great successes in computer vision applications such as classification [5], denoising [6], [7], [8], segmentation [9], and super-resolution [10], etc.

In medical imaging, deep learning approaches have been extensively used for image-based diagnosis. However, deep learning approaches for medical image reconstruction problems such as X-ray CT reconstruction are relatively less studied, although some preliminary results are available [11], [12]. In particular, our group has introduced the world-first deep learning approach for low-dose X-ray CT [11], whose performance has been rigorously confirmed by winning the second place award in 2016 AAPM Low-Dose CT Grand Challenge. However, the reconstruction results tend to lose some fine detail textures of the original images.

Therefore, one of the important contributions of this paper is to propose a drastically improved deep network that overcomes the limitations of previous work by maintaining detailed textures and edges. The key to the improvement comes from our novel observation that the CNN in [11] can be interpreted as a special form of *deep convolutional framelets* [13]. Here, deep convolutional framelets is a recent proposal of signal representation by recursively applying the convolutional framelet expansion by Yin et al [14] combined with the rectified linear unit (ReLU) nonlinearity, which can be designed to achieve perfect reconstruction (PR). Specifically, the original convolutional framelets [14] is a tight frame representation of a signal by convolving data-driven local basis with a given nonlocal basis. The convolutional framelets has an intriguing link to recent low rank Hankel matrix approaches [15], [16], [17], [18], [19], [20], [21], since the optimal bases can be obtained from the Hankel matrix decomposition [14]. In our companion paper [13], we further revealed that the non-local and local basis structure of convolutional framelets has a close link to deep learning network by observing that the non-local basis determines the overall deep network architecture, for which the local basis can be learned optimally as convolutional filters.

Seeing with the new eyes of deep convolutional framelets, this paper discovers the limitation of our prior work for low-dose X-ray CT [11] and provides a new theory for performance improvement. In particular, we show that 1) a deep convolutional framelets expansion is still possible if redundant non-local transform is applied beforehand to decorrelate the global redundancies, and 2) the deep convolutional framelets allows a novel signal boosting scheme by combining the multiple signal representation. This observation leads to a novel wavelet domain residual learning (WavResNet) algorithm with redundant

Authors are with the Department of Bio and Brain Engineering, Korea Advanced Institute of Science and Technology (KAIST), Daejeon 34141, Republic of Korea (e-mail: {eunheekang,jaejun2004,jong.ye}@kaist.ac.kr).

Part of this work was presented in 2017 International Conference on Fully Three-Dimensional Image Reconstruction in Radiology and Nuclear Medicine.

wavelet transform and signal boosting, which shows significant improvement compared to the prior work [11].

II. THEORY

A. Notations

The notation $0_{p \times q}$ means the $p \times q$ zero matrix. The $n \times n$ identity matrix is referred to as $I_{n \times n}$. For a given matrix $A \in \mathbb{R}^{m \times n}$, the notation A^\dagger refers to the generalized inverse. The superscript \top of A^\top denotes the Hermitian transpose. Because we are mainly interested in real valued cases, \top is equivalent to the transpose T . The inner product in matrix space is defined by $\langle A, B \rangle = \text{Tr}(A^\top B)$, where $A, B \in \mathbb{R}^{n \times m}$. For a matrix A , $\|A\|_F$ denotes its Frobenius norm. For a given matrix $C \in \mathbb{R}^{n \times m}$, c_j denotes its j -th column, and c_{ij} is the (i, j) elements of C . If a matrix $\Psi \in \mathbb{R}^{p \times d \times q}$ is partitioned as $\Psi = [\Psi_1^\top \cdots \Psi_p^\top]^\top$ with sub-matrix $\Psi_i \in \mathbb{R}^{d \times q}$, then ψ_j^i refers to the j -th column of Ψ_i .

B. Hankel Matrix Representation of Convolution

Convolution operation in CNN can be represented using Hankel matrix operation. Specifically, a (wrap-around) Hankel matrix can be easily obtained from (circular) convolution [15]. In this paper, to avoid special treatment of boundary condition, our theory is mainly derived using circular convolution. Specifically, let $f = [f[1], \dots, f[n]]^T \in \mathbb{R}^n$ and $\psi = [\psi[1], \dots, \psi[d]]^T \in \mathbb{R}^d$ be an input image and a convolutional filter kernel. Then, a single-input single-output (SISO) convolution is given by a matrix vector multiplication:

$$y = f \circledast \psi = \mathbb{H}_d(f) \psi, \quad (1)$$

where $\mathbb{H}_d(f)$ is a wrap-around Hankel matrix

$$\mathbb{H}_d(f) = \begin{bmatrix} f[1] & f[2] & \cdots & f[d] \\ f[2] & f[3] & \cdots & f[d+1] \\ \vdots & \vdots & \ddots & \vdots \\ f[n] & f[1] & \cdots & f[d-1] \end{bmatrix}.$$

Similarly, a single-input multi-output (SIMO) convolution using d -length filters $\psi_1, \dots, \psi_q \in \mathbb{R}^d$ can be represented by

$$Y = f \circledast \Psi = \mathbb{H}_d(f) \Psi \quad (2)$$

where

$$Y := [y_1 \cdots y_q] \in \mathbb{R}^{n \times q}, \quad \Psi := [\psi_1 \cdots \psi_q] \in \mathbb{R}^{d \times q},$$

and q denotes the number of output channels. Multi-input multi-output (MIMO) convolution is defined by

$$y_i = \sum_{j=1}^p f_j \circledast \psi_j^i, \quad i = 1, \dots, q \quad (3)$$

where p and q are the number of input and output channels, respectively; $\psi_j^i \in \mathbb{R}^d, i = 1, \dots, q; j = 1, \dots, p$ refer to

the corresponding filters with the filter length d . Then, the corresponding matrix representation is given by

$$\begin{aligned} Y &= F \circledast \Psi \\ &= \sum_{j=1}^p \mathbb{H}_d(f_j) \Psi_j \\ &= \mathbb{H}_{d|p}([f_1 \cdots f_p]) \begin{bmatrix} \Psi_1 \\ \vdots \\ \Psi_p \end{bmatrix} \end{aligned} \quad (4)$$

where $\mathbb{H}_{d|p}([f_1 \cdots f_p])$ is an *extended Hankel matrix* by stacking p Hankel matrices side by side:

$$\mathbb{H}_{d|p}([f_1 \cdots f_p]) := [\mathbb{H}_d(f_1) \quad \mathbb{H}_d(f_2) \quad \cdots \quad \mathbb{H}_d(f_p)] \quad (5)$$

and

$$\Psi_j = [\psi_1^j \cdots \psi_q^j] \in \mathbb{R}^{d \times q}.$$

C. Convolutional Framelets

The convolutional framelets by Yin et al [14] is a novel signal representation scheme using two bases: fixed non-local basis and data-driven learning-based local dictionaries, which is related to a decomposition of the aforementioned Hankel matrices. This results in energy compacting expansion coefficients if the underlying Hankel matrix has low dimensional structure [14]. Then, an image denoising problem can be addressed by retaining the high energy expansion coefficients.

In order to reveal the link between the convolutional framelets and deep network, we have significantly extend the original form of the convolutional framelets [13] as follows:

Proposition 2.1 ([13]). *Let $\Phi, \tilde{\Phi} \in \mathbb{R}^{n \times m}$ and $\Psi, \tilde{\Psi} \in \mathbb{R}^{d \times q}$ satisfy the following resolution of identity:*

$$\tilde{\Phi} \Phi^\top = I_{n \times n}, \quad \Psi \tilde{\Psi}^\top = I_{d \times d}, \quad (6)$$

Then, for any n -dimensional vector $f \in \mathbb{R}^n$,

$$\begin{aligned} f &= \mathbb{H}_d^\dagger \left(\tilde{\Phi} (\Phi^\top \mathbb{H}_d(f) \Psi) \tilde{\Psi}^\top \right) \\ &= \frac{1}{d} \sum_{i=1}^m \sum_{j=1}^q \langle f, \phi_i \circledast \psi_j \rangle \tilde{\phi}_i \circledast \tilde{\psi}_j, \end{aligned} \quad (7)$$

or equivalently,

$$f = \frac{1}{d} \sum_{i=1}^m \left(\tilde{\Phi} c_j \right) \circledast \tilde{\psi}_j, \quad (8)$$

where c_j is the j -th column of the framelet coefficient matrix

$$\begin{aligned} C &= \Phi^\top (f \circledast \Psi) \\ &= \begin{bmatrix} \langle f, \phi_1 \circledast \psi_1 \rangle & \cdots & \langle f, \phi_1 \circledast \psi_q \rangle \\ \vdots & \ddots & \vdots \\ \langle f, \phi_m \circledast \psi_1 \rangle & \cdots & \langle f, \phi_m \circledast \psi_q \rangle \end{bmatrix} \in \mathbb{R}^{m \times q}. \end{aligned} \quad (9)$$

and ϕ_j and ψ_j denote the j -th column of Φ and Ψ , respectively.

The condition to enable the decomposition (7) is often referred to as *perfect reconstruction (PR) condition*. Here, the column of the local basis Ψ and $\tilde{\Psi}$ are often referred to as

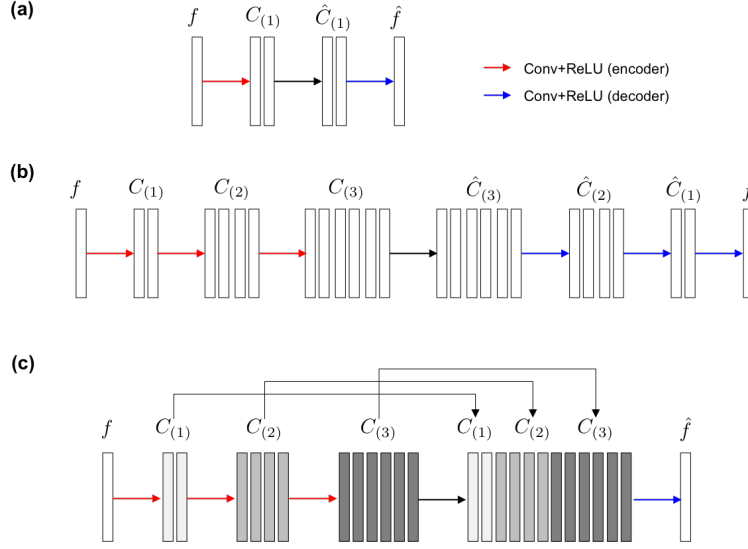


Fig. 1. (a) Single-layer encoder-decoder architecture, (b) multi-layer encoder-decoder architecture, and (c) the corresponding boosting network architecture using a concatenation layer.

local filters and its dual filters. In addition, Φ^\top is a non-local transform that further de-correlates the filtered signals by local filters Ψ . In (9), it is important to note that the order of local filter and the global filters can not be interchanged, because matrix multiplication does not commute with convolution. This issue will be revisited later.

One of the most important discoveries in our companion paper [13] is that the structure in (8) and (9) are closely related to the convolutional layers in CNN. More specifically, the single layer convolutional framelet expansion can be represented by

$$C^{(1)} = \Phi^\top (f \otimes \Psi) \quad (10)$$

$$f = \frac{1}{d} \sum_{i=1}^m (\tilde{\Phi} c_j) \otimes \tilde{\psi}_j = (\Phi C^{(1)}) \otimes \tau(\tilde{\Psi}) \quad (11)$$

where

$$\tau(\tilde{\Psi}) := \frac{1}{d} \begin{bmatrix} \tilde{\psi}_1 \\ \vdots \\ \tilde{\psi}_q \end{bmatrix}. \quad (12)$$

If $\Phi = I_{n \times n}$, this corresponds to the encoder and decoder network without pooling as shown in Fig. 1(a). Moreover, the popular pooling and unpooling can be explained by choosing appropriated the non-local basis Φ and $\tilde{\Phi}$ [13]. However, we also showed that the pooling and unpooling are non-local bases that do not satisfy the perfect reconstruction condition (PR) [13]. Thus, we proposed a Haar wavelet basis to improve upon the existing deep learning architecture [13].

In our companion paper [13], this idea is further extended to enable convolutional framelets decomposition of multiple inputs using redundant bases. Specifically, Let $\Phi, \tilde{\Phi} \in \mathbb{R}^{n \times m}$ and $\Psi, \tilde{\Psi} \in \mathbb{R}^{pd \times q}$ satisfy the resolution of identity, i.e. $\tilde{\Phi} \Phi^\top = I_{n \times n}$, $\Psi \tilde{\Psi}^\top = I_{pd \times pd}$. Suppose, furthermore, that

$$\Psi^\top = [\Psi_1^\top \ \cdots \ \Psi_p^\top], \quad \tilde{\Psi}^\top = [\tilde{\Psi}_1^\top \ \cdots \ \tilde{\Psi}_p^\top]$$

with $\Psi_i, \tilde{\Psi}_i \in \mathbb{R}^{d \times q}$, whose j -th column is represented by ψ_j^i and $\tilde{\psi}_j^i$, respectively. Then, for any matrix $Z \in \mathbb{R}^{n \times p}$, we have

$$Z =$$

$$\frac{1}{d} \sum_{i,j,k=1}^{m,q,p} \begin{bmatrix} \langle z_k, \phi_i \otimes \psi_j^k \rangle \tilde{\phi}_i \otimes \tilde{\psi}_j^1 & \cdots & \langle z_k, \phi_i \otimes \psi_j^k \rangle \tilde{\phi}_i \otimes \tilde{\psi}_j^p \end{bmatrix} \quad (13)$$

or equivalently,

$$\begin{aligned} Z &= \frac{1}{d} \left[\sum_{j=1}^q (\tilde{\Phi} c_j) \otimes \tilde{\psi}_j^1 \ \cdots \ \sum_{j=1}^q (\tilde{\Phi} c_j) \otimes \tilde{\psi}_j^p \right] \\ &= (\Phi C) \otimes \tau(\tilde{\Psi}) \end{aligned} \quad (14)$$

where

$$\tau(\tilde{\Psi}) := \frac{1}{d} \begin{bmatrix} \tilde{\psi}_1^1 & \cdots & \tilde{\psi}_1^p \\ \vdots & \ddots & \vdots \\ \tilde{\psi}_q^1 & \cdots & \tilde{\psi}_q^p \end{bmatrix} \in \mathbb{R}^{dq \times p} \quad (15)$$

and

$$\begin{aligned} C &= \Phi^\top (Z \otimes \Psi) \\ &= \sum_{k=1}^p \begin{bmatrix} \langle z_k, \phi_1 \otimes \psi_1^k \rangle & \cdots & \langle z_k, \phi_1 \otimes \psi_q^k \rangle \\ \vdots & \ddots & \vdots \\ \langle z_k, \phi_m \otimes \psi_1^k \rangle & \cdots & \langle z_k, \phi_m \otimes \psi_q^k \rangle \end{bmatrix} \end{aligned} \quad (16)$$

D. Deep Convolutional Framelets Neural Network

The resulting convolutional framelet expansion (14) and (16) are indeed MIMO convolution operations. Thus, by combining with (10) and (11), this suggests that the convolutional framelets can be extended to a deep network if multiple convolutional framelet expansions are cascaded sequentially while retaining the encoder-decoder architecture (see Fig. 1(b)).

In general, the l -layer implementation of the convolutional framelets is given by

$$g \left(C^{(l)}; \{\tilde{\Psi}^{(j)}\}_{j=1}^l \right)$$

$$\begin{aligned}
&= \mathbb{H}_{d_{(1)}|p_{(1)}}^\dagger \left(\cdots \left(\mathbb{H}_{d_{(l)}|p_{(l)}}^\dagger \left(C^{(l)} \tilde{\Psi}^{(l)\top} \right) \right) \cdots \tilde{\Psi}^{(1)\top} \right) \\
&= C^{(l)} \otimes \tau(\tilde{\Psi}^{(l)}) \otimes \tau(\tilde{\Psi}^{(l-1)}) \cdots \otimes \tau(\tilde{\Psi}^{(1)}) \quad (17)
\end{aligned}$$

with the encoder layer

$$\begin{aligned}
C^{(l)} &:= C \left(Tf; \{\Psi^{(j)}\}_{j=1}^l \right) \\
&= \mathbb{H}_{d_{(l)}|p_{(l)}} \left(\cdots \left(\mathbb{H}_{d_{(1)}|p_{(1)}} (Tf) \Psi^{(1)} \right) \cdots \Psi^{(l)} \right) \\
&= (Tf) \otimes \Psi^{(1)} \otimes \Psi^{(2)} \cdots \otimes \Psi^{(l)} \quad (18)
\end{aligned}$$

where $d_{(i)}$ and $p_{(i)}$ denotes the filter length and the number of input channels at the i -th layer, respectively.

Then, with the given input and target sample pairs $\{f_i, y_i\}_{i=1}^N$ as a training data and by inserting the rectified linear unit (ReLU) nonlinearity $\rho(x) = \max\{0, x\}$ in some steps of the convolutions in (17) and (18), the L -layer convolutional framelets training problem is given by

$$\min_{\{\Psi^{(j)}, \tilde{\Psi}^{(j)}\}} \sum_{i=1}^N \left\| y_i - g \left(C^{(L)}; \{\tilde{\Psi}^{(j)}\}_{j=1}^L \right) \right\|^2 \quad (19)$$

where $g(\cdot)$ is defined by (17). While this is very similar to the existing CNN training, there exists fundamental differences. First, even with the ReLU nonlinearity, we show that the PR is still guaranteed if sufficient number of filter channels are available [13]. In this case, if the target sample y_i is the same as the input f_i , the training problem is nothing but the filter bank design problem to guarantee the PR.

In fact, deep convolutional framelets provide answers to many important open questions in deep learning [13]:

- 1) number of filter channels in convolutional layer,
- 2) role of rectified linear unit (ReLU),
- 3) role of pooling and unpooling,
- 4) role of by-pass connection or residual network.

In [13], we further show that the lower layers perform signal decomposition using various filter bank satisfying the PR conditions, after which high layers of deep network exploit the low-rank approximation of extended Hankel matrix from multiple channel images. Since the low-rank approximation of Hankel matrix is very powerful tool for inverse problems[15], [16], [17], [18], [19], [20], [21], we conjecture that a deep network is trained such that the signal decomposition as well as Hankel matrix approximation is optimally fitted to the desired input/output relationship.

E. Convolutional Framelets with Global Transform

In this section, we further extend the results of [13] so that non-local global transform is applied first, after which the local (and often additional non-local) filtering is applied to remove the remaining local correlations. The new architecture has many advantages compared to the aforementioned deep convolutional framelets architecture in [13] that applies the local filtering first. More specifically, if the global transform is applied first, we do not need to backpropagate the gradient through the global transform, so more sophisticated global transform can be used to exploit the global redundancies.

In order to have the best denoising performance, the convolutional framelet should have good energy compaction property [14]. Thus, we are interested in using contourlet transform without decimation [22] by following our prior work [11]. Due to the vanishing moments of wavelets, the wavelet transform can annihilate the smoothly varying signals while maintaining the image edges, thus resulting in good energy compaction. Furthermore, low-dose X-ray CT images exhibit streaking noise. Therefore, the contourlet transform [22] is good for detecting the streaking noise patterns and expands the directional edge information of X-ray CT images with high energy compaction.

Mathematically, for a given signal $f \in \mathbb{R}^n$, the directional subband transform $\{T_k\}_{k=1}^p, T_k \in \mathbb{R}^{n \times n}$ in contourlet transform satisfies the resolution of identity:

$$\sum_{k=1}^p \tilde{T}^{(k)\top} T^{(k)} = I_{n \times n}, \quad (20)$$

which implies that there exists inverse transform $\{\tilde{T}_k\}_{k=1}^p$ to collect the each subband signals to recompose the original signal. Specifically, the signal f can be decomposed into directional components:

$$f = \sum_{k=1}^p \tilde{T}^{(k)\top} T^{(k)} f = \sum_{k=1}^p \tilde{T}^{(k)\top} f_k$$

where $f_k = T^{(k)} f \in \mathbb{R}^n$ corresponds to the k -th subband signals.

Note that the role of global transform $T^{(k)}$ and the nonlocal basis Φ^\top in deep convolutional framelets are similar, since they both de-correlate the global redundancies. Thus, this paper only uses the $T^{(k)}$ by setting $\Phi^{(k)} = I_{n \times n}, \forall k$. Then, our goal is to obtain the convolutional framelet representation of the input matrix

$$Tf := [T^{(1)}f \quad \cdots \quad T^{(p)}f].$$

In this case, by inserting Tf in (14), we have

$$\begin{aligned}
Tf &= \frac{1}{d} \left[\sum_{j=1}^q c_j \otimes \tilde{\psi}_j^1 \quad \cdots \quad \sum_{j=1}^q c_j \otimes \tilde{\psi}_j^p \right] \\
&= C \otimes \tau(\tilde{\Psi}) \quad (21)
\end{aligned}$$

where $\tau(\tilde{\Psi})$ is defined by (15) and C denotes the framelet coefficient matrix

$$C = (Tf) \otimes \Psi. \quad (22)$$

After the first layer using Tf , the successive layers are similar implemented using the filtered multi-channel signals.

F. Boosting using multiple signal representation

Another important contribution of this paper is the theory for signal boosting using multiple signal representation. More specifically, the PR conditions for deep convolutional framelets

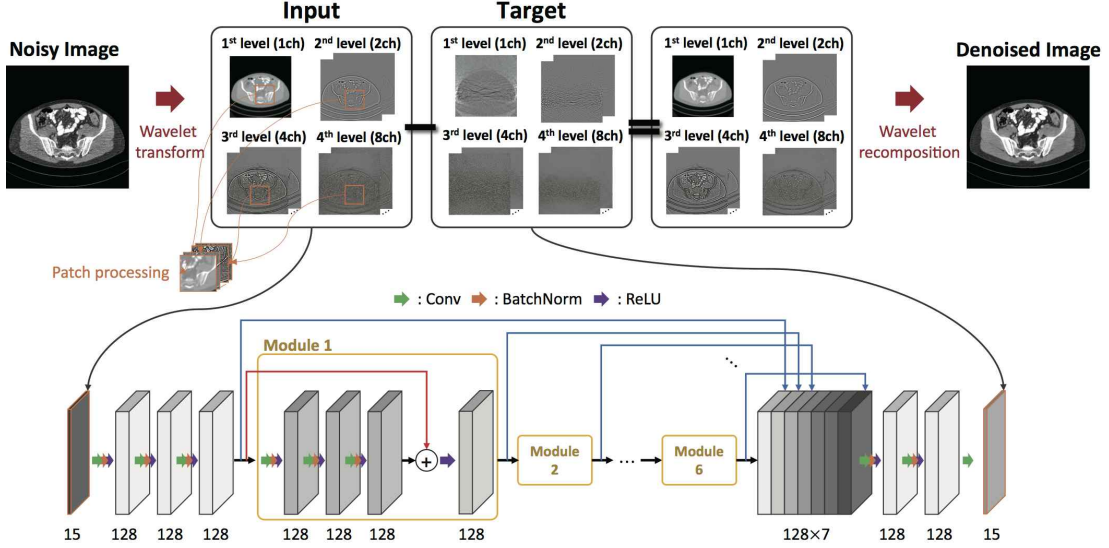


Fig. 2. The proposed WavResNet architecture for low-dose X-ray CT reconstruction.

up to L -layer can be written by

$$\begin{aligned}
 Tf &= \mathbb{H}_{d(1)|p(1)}^\dagger \left(C^{(1)} \tilde{\Psi}^{(1)\top} \right) \\
 &= C^{(1)} \otimes \tau \left(\tilde{\Psi}^{(1)} \right) \\
 &\vdots \\
 Tf &= \mathbb{H}_{d(1)|p(1)}^\dagger \cdots \left(\mathbb{H}_{d(L)|p(L)}^\dagger \left(C^{(L)} \tilde{\Psi}^{(L)} \right) \cdots \tilde{\Psi}^{(1)} \right) \\
 &= C^{(L)} \otimes \tau \left(\tilde{\Psi}^{(L)} \right) \cdots \otimes \tau \left(\tilde{\Psi}^{(1)} \right)
 \end{aligned}$$

Thus, for a given intermediate encoder output $\{C^{(l)}\}_{l=1}^L$, by denoting $h^{(l)} := \tau \left(\tilde{\Psi}^{(l)} \right) \cdots \otimes \tau \left(\tilde{\Psi}^{(1)} \right)$ the decoder can be constructed by combining multi-input single output convolution from multiple representation:

$$Tf = \sum_{i=1}^L w_i C^{(i)} \otimes h^{(i)}, \quad \text{where } \sum_{i=1}^L w_i = 1 \quad (23)$$

More specifically, this procedure can be described by one step filtering of concatenated encoder outputs as shown in Fig. 1(c).

III. METHOD

A. Proposed network architecture

The resulting WavResNet is illustrated in Fig. 2. Here, we first apply non-subsampled contourlet transform, which is composed of two steps [22]. First step is a non-decimated multi-scale decomposition to produce highpass and lowpass subbands, and the second step is a directional decomposition to divide the highpass subband into directional components. The k -th level filter banks are generated by iterating these two steps. There is no down-sampling or up-sampling in the filter banks; thus, it is a shift invariant. We used 4 level decomposition and 8, 4, 2, 1 directional separations for each level, which produces the total 15 bands. Thus, we have 15 non-local transforms $T^{(k)}$, $k = 1, \dots, 15$. As shown on the upper part of Fig. 2, rather than estimating the noise-free images, our network estimates the noises. This is indeed

equivalent to the bypass connection or residual net [13]. Once the residual wavelet coefficients are estimated, denoised contourlet coefficients are obtained by subtracting them from the input noisy contourlet coefficients.

The architecture of the deep neural network is shown in the lower part of Fig. 2. The first convolution layer uses 128 set of $3 \times 3 \times 15$ convolution kernels to produce 128 channel feature maps. This corresponds to $p(1) = 15, d(1) = 9$, so the number of minimum output channels to satisfy PR is $q(1) = 15 \times 9 = 135$. Moreover, with the ReLU, this increases up to $135 \times 2 = 270$ (see [13] for this calculation), which is bigger than 128 channels. Thus, the first layer performs an approximation of the first layer Hankel matrix. Then, the following convolution layers use two $3 \times 3 \times 128$ convolution kernels, which is again believed to perform Hankel matrix approximation. Next, we have 6 set of main module composed of 3 sets of convolution, batch normalization, and ReLU layers, and 1 bypass connection with a convolution and ReLU layer. Again, this exploits the advantages of residual learning in deep convolutional framelet [13].

One of the uniquenesses of the WavResNet is that it has the concatenation layer as shown in Fig. 1(c). Specifically, WavResNet concatenates the outputs of the individual modules, which is followed by the convolutional composed of 128 set of $3 \times 3 \times 896$ convolution kernels. As discussed before, this corresponds to the signal boosting using multiple signal representation. In optimization aspect, this also provides various paths for gradient back-propagation. Finally, the last convolution layer uses 15 sets of $3 \times 3 \times 128$ convolution kernels. This may correspond to the pair-wise decoder layers with respect to the first two convolutional layers.

B. Network training

We applied stochastic gradient descent (SGD) optimization method to train the proposed network. The shift invariant contourlet transform allows the patch processing and we used

$55 \times 55 \times 15$ patches for the training. The size of mini-batch was 10. The convolution kernels were initialized by random Gaussian distribution. The learning rate was initially set to 0.01 and decreased continuously down to 10^{-5} . The gradient clipping was employed in the range $[-10^{-3}, 10^{-3}]$ to use a high learning rate in the initial steps for the fast convergence. For data augmentation, the training data were randomly flipped horizontally and vertically. Our network was implemented using MatConvNet [23] in MATLAB 2015a environment (Mathworks, Natick).

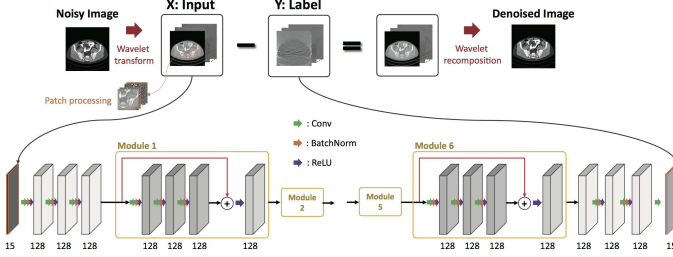


Fig. 3. A symmetric network architecture to investigate the importance of boosting layers in WavResNet.

C. Training dataset

We used projection data obtained from “2016 Low-Dose CT Grand Challenge”. The raw projection data were measured by a 2D cylindrical detector that moves along a helical trajectory using a z-flying focal spot [24]. These projections were approximated into fanbeam projection data by a single slice rebinning technique [25]. We reconstructed X-ray CT images using conventional filtered backprojection algorithm. The number of pixels in X-ray CT images is 512×512 and the slice thickness is 3mm. We have 9 patient data sets of routine dose and quarter dose data for the training. Eight patient data were used for the training and validation, and the remaining one patient data was used for testing. Among the eight patient data, we used 3236 slices for the training and the remaining 350 slices for the validation.

D. Baseline algorithms

For a quantitative evaluation, we use the image metrics such as peak signal-to-noise ratio (PSNR) and structural similarity (SSIM) index. The mean square error (MSE), which is defined as

$$MSE = \frac{1}{mn} \sum_{i=0}^{m-1} \sum_{j=0}^{n-1} [Y(i, j) - X(i, j)]^2, \quad (24)$$

where X is the reconstruction image and Y is a noise-free (ground truth) image. The PSNR is defined in terms of MSE,

$$PSNR = 10 \cdot \log_{10} \left(\frac{MAX_Y^2}{MSE} \right) \quad (25)$$

$$= 20 \cdot \log_{10} \left(\frac{MAX_Y}{\sqrt{MSE}} \right), \quad (26)$$

where MAX_Y is the maximum value of image Y . SSIM is measured image degradation as perceived change in structural information [26] and it is defined as

$$SSIM = \frac{(2\mu_X\mu_Y + c_1)(2\sigma_{XY} + c_2)}{(\mu_X^2 + \mu_Y^2 + c_1)(\sigma_X^2 + \sigma_Y^2 + c_2)}, \quad (27)$$

where μ_X is a average of X , σ_X^2 is a variance of X and σ_{XY} is a covariance of X and Y . There are two variables to stabilize the division such as $c_1 = (k_1 L)^2$ and $c_2 = (k_2 L)^2$. L is a dynamic range of the pixel intensities. k_1 and k_2 are constants by default $k_1 = 0.01$ and $k_2 = 0.03$. The routine dose X-ray CT images were used to the ground truth and the denoised X-ray CT images from quarter dose were used to calculate the image metrics.

We compared the proposed method with the other denoising algorithms such as BM3D [27], MBIR regularized by total variation (TV), and the recent image domain deep learning approach (RED-CNN) [12]. MBIR regularized by TV was solved using an alternative direction method of multiplier (ADMM) [3] and Chambolle’s proximal TV [28]. The parameters of RED-CNN were obtained from the original paper [12].

To verify the improvement of the new algorithm, we perform comparative study with our previous deep network in wavelet domain for “2016 Low-Dose CT Grand Challenge” [11]. We call this network as AAPM-Net. The main difference between the proposed one and the AAPM-Net comes from the definition of the target images. In AAPM-Net, the target images was the original wavelet coefficients except the lowest frequency band. More specifically, in AAPM-Net, the lowest frequency band target is the residual, whereas the higher frequency band signals are the wavelet coefficients themselves. Therefore, this is not a residual net from the perspective of deep convolutional framelets. On the other hand, in WavResNet, the residual wavelet coefficients between the routine-dose and low-dose inputs are estimated for every subband.

In order to demonstrate the importance of signal boosting, we also implemented a symmetric network as illustrated in Fig. 3. Except for the concatenation layers, the symmetric network also has identical 6 modules structures with symmetric encoder and decoder structures. To have fair comparison, the symmetric network also estimates the residual wavelet coefficients between the routine-dose and low-dose inputs.

IV. EXPERIMENTAL RESULT

A. Comparison with AAPM-Net

To confirm the improvement over the AAPM-Net, we present the reconstruction images of one patient data in the test data set (see Fig. 4, 5 and 6). This data have routine-dose images that can be used for subjective evaluation and objective evaluation using PSNR, and SSIM.

In Fig. 4, various kinds of slices such as liver and pelvic bones are described and the magnified images are expressed in the yellow boxes. In AAPM-Net results, noise level was significantly reduced, but the results are blurry and loses some details. On the other hand, the result of the proposed WavResNet clearly shows that the improved noise reduction while maintaining the edge details and the textures which

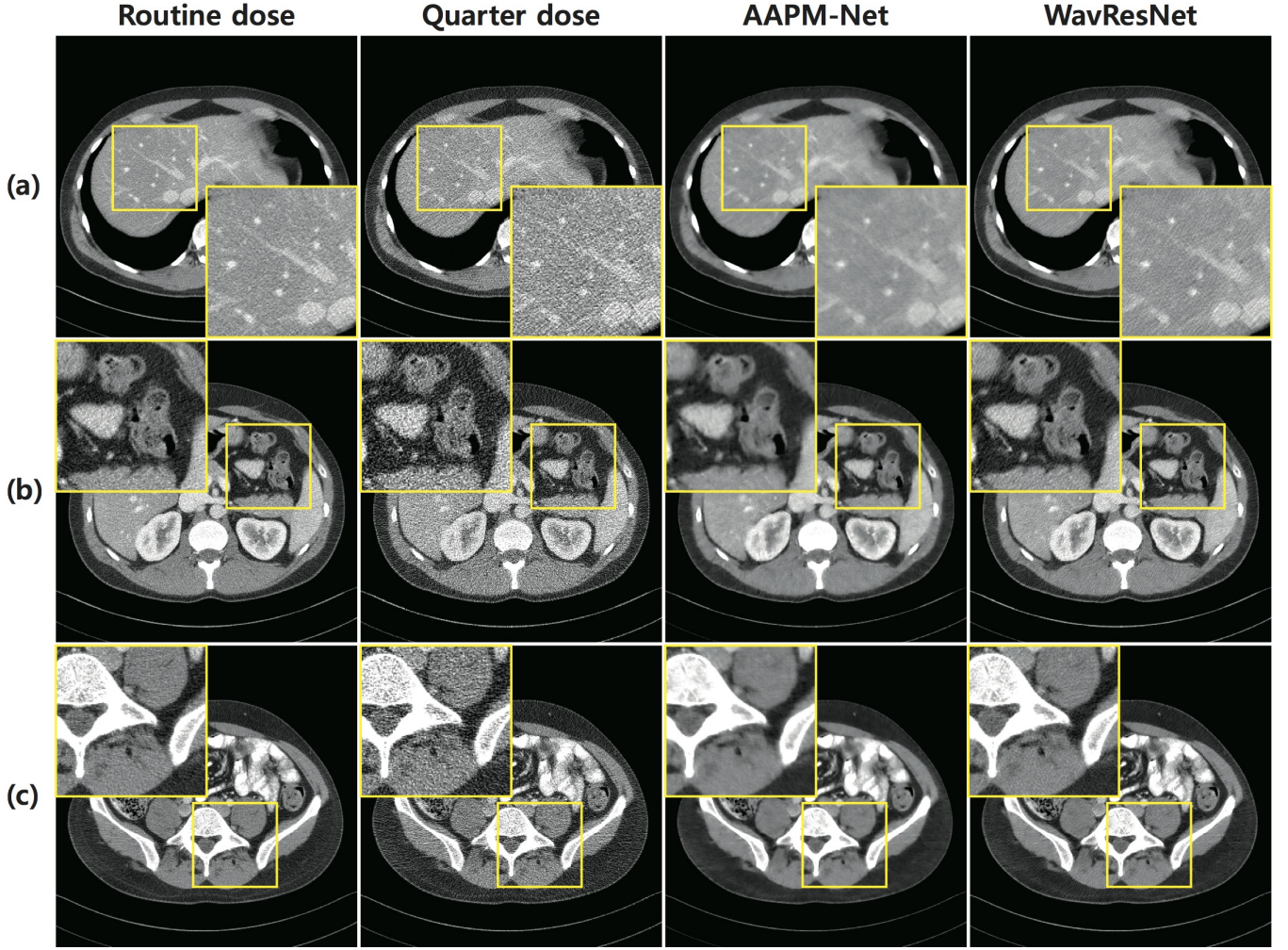


Fig. 4. Transverse view reconstruction results with routine-dose and quarter-dose images. AAPM-Net is the algorithm which we applied to the “2016 Low-Dose CT Grand Challenge”. Intensity range is $(-160, 240)$ [HU] (Hounsfield Unit). (a) Example of liver, (b) example of intestine and (c) example of pelvic bone.

is helpful for diagnostic purpose. More specifically, for the case of an liver image in Fig. 4 (a), the WavResNet result retains the fine details such as vessels in the liver and it has better sharpness than the AAPM-Net. In Fig. 4 (b), the detail of internal structure of intestine was not observed in quarter-dose images and AAPM-Net results, while they are well-recovered in WavResNet. To examine the streaking noise reduction ability, we presented the slice which has the pelvic bone in Fig. 4 (c). WavResNet is again good at preserving the edge details such as inside region of the bones and the texture of the organ which located between the bones, while the streaking artifacts were completely removed. The coronal and sagittal view of the reconstruction results are described in Fig. 5. The quarter-dose images show that the noise levels are different depending on the slices. The lower part of the images exhibit a high noise level because the pelvic bones are included. The proposed method can remove a wide range of noise levels and maintain the texture and edge information.

The difference images between the result images and routine-dose images in Fig. 6 confirm the superiority of the wavelet domain deep convolutional framelets with residual

network. Each column describes the slice in Fig. 4 (a) and (c), respectively. The difference images of symmetric network and WavResNet only contains the noise of low-dose X-ray CT images, while the difference images of AAPM-Net also contains the edge information.

B. Comparison with existing algorithms

Fig. 7 shows the results by the comparative algorithms such as BM3D [27], MBIR regularized by TV, and RED-CNN [12]. BM3D is a state-of-art of image denoising algorithm using nonlocal patch processing, and MBIR is currently a standard algorithm of low-dose X-ray CT images. RED-CNN is recently proposed deep network for low-dose X-ray CT.

The intensity of the transverse view in Fig. 7 is adjusted to see inside structures of the lung. The result of BM3D loses the details in the lung such as vessels and exhibited some cartoon artifact. The result of MBIR appears a little blurred and textures are reconstructed incorrectly. On the other hand, deep learning based denoising algorithms have better performances than the other algorithms. However, RED-CNN results are somewhat blurry, while the proposed method provides clear

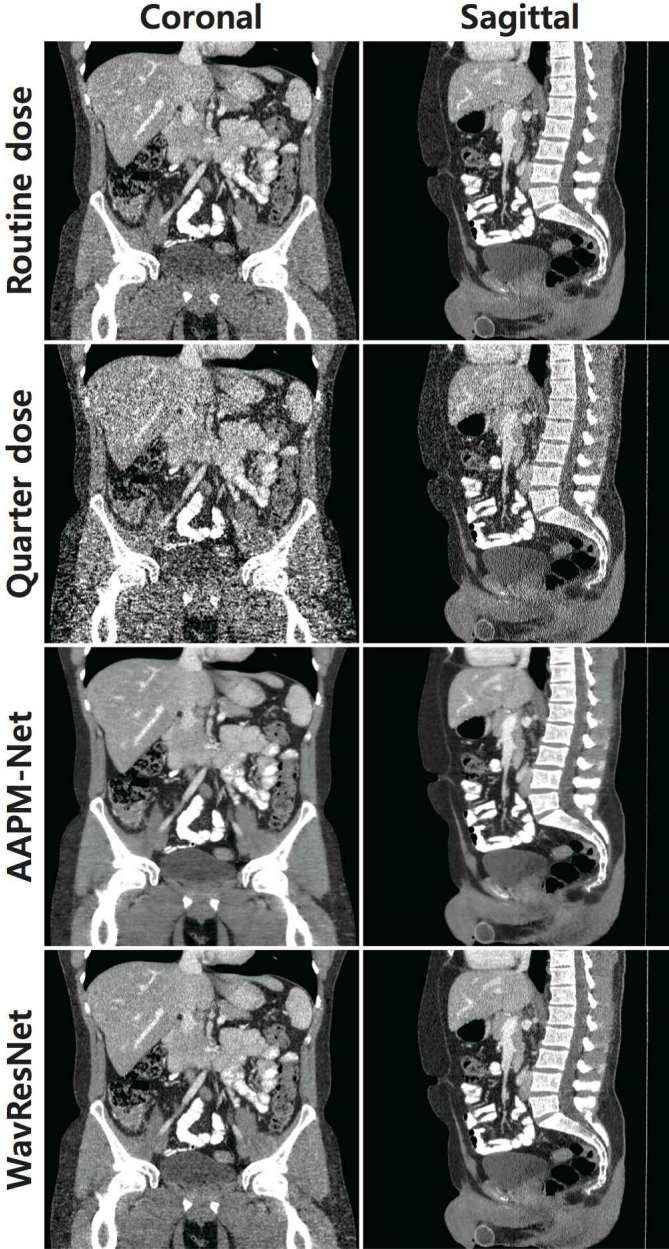


Fig. 5. Coronal and sagittal view reconstruction results with routine-dose and quarter-dose images. AAPM-Net is the algorithm which we applied to the “2016 Low-Dose CT Grand Challenge”. Intensity range is $(-160, 240)$ [HU].

reconstruction results. The coronal and sagittal view of the results further confirmed the performance of the WavResNet. In the lower part of the coronal and sagittal view images have the higher noise level because of the pelvic bones. The results of BM3D, MBIR and RED-CNN still have noises between the pelvic bones and exhibited blurry images between the pelvic bones, whereas the proposed method has clear results with significantly reduced noise levels.

Table I presents the averaged PSNR and SSIM index values of the results from 486 slices. The proposed method has the highest PSNR and SSIM index value. Symmetric network’s PSNR and SSIM values are slightly lower than the proposed method. While the difference images of symmetric network

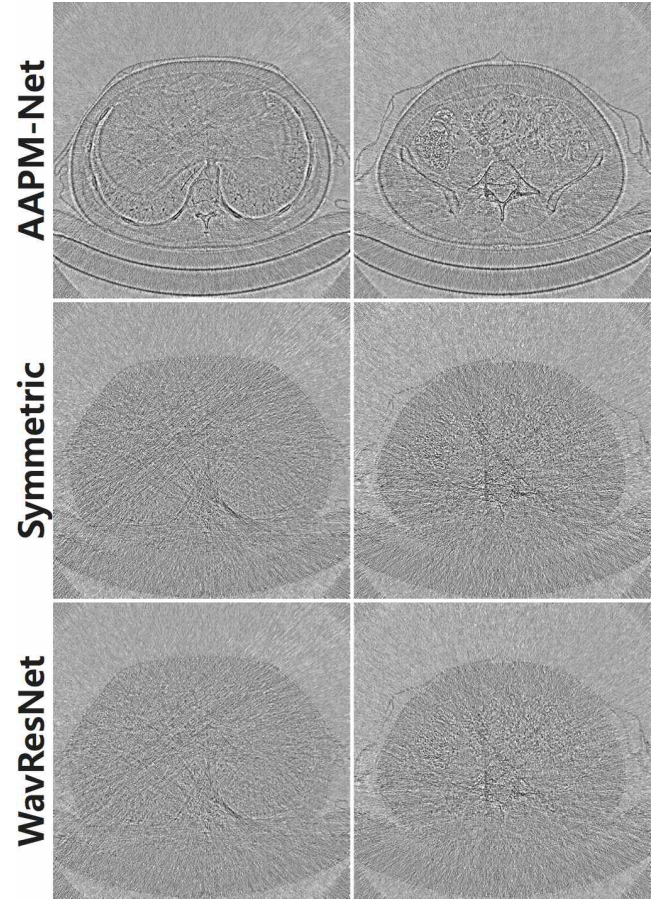


Fig. 6. Difference images between reconstruction images and routine dose image. Each column images are same slices the row of Fig. 4. Intensity range is $(-1100, 950)$ [HU].

TABLE I
COMPARISON OF LOW-DOSE X-RAY CT RECONSTRUCTION ALGORITHMS

	PSNR [dB]			SSIM index		
	1st half	2nd half	overall	1st half	2nd half	overall
Quarter-dose	32.64	32.39	32.51	0.726	0.749	0.738
BM3D	37.47	37.59	37.53	0.855	0.874	0.865
MBIR TV	36.49	36.68	36.58	0.800	0.826	0.813
RED-CNN	37.56	37.74	37.65	0.881	0.896	0.888
Symmetric	37.78	38.32	38.05	0.868	0.891	0.879
Proposed	38.05	38.41	38.23	0.886	0.904	0.895

and the proposed method look similar, the quantitative improvement in the image metric values clearly confirms the advantages of signal boosting effect via concatenation layer.

To quantitatively evaluate the convergence behaviour and reconstruction performance, WavResNet was compared with other baseline network that has identical structure but directly estimate the wavelet coefficients. Fig. 8 confirms that the learning performance of WavResNet is the best. Here, we also showed the AAPM-Net results. WavResNet has about 1dB improvement in PSNR over AAPM-Net.

With regard to the computation, the CNN framework is ad-

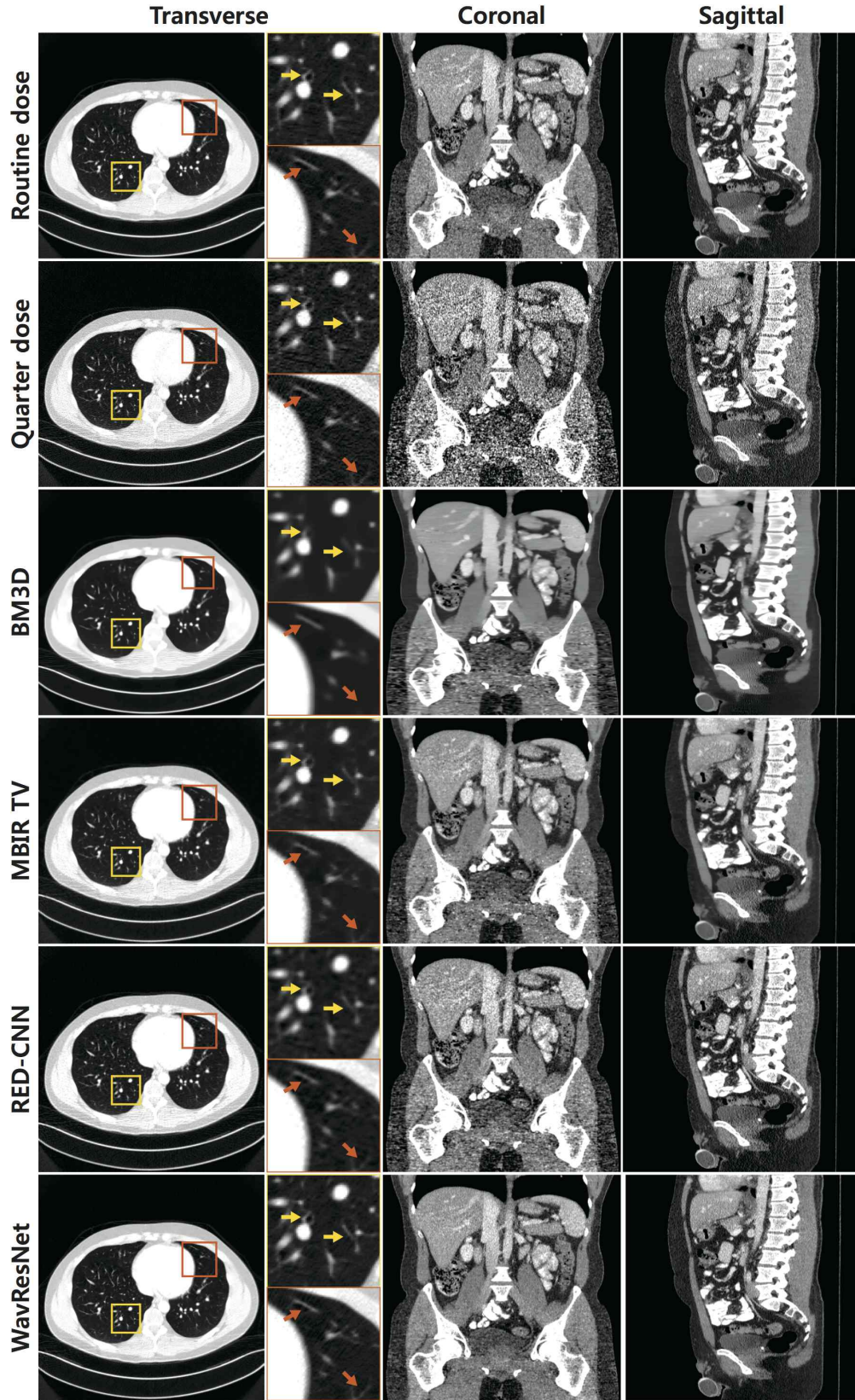


Fig. 7. Reconstruction results with routine-dose and quarter-dose image. Transverse view reconstruction images' intensity range is adjusted to see the details in the lung. Intensity range is $(-1000, 100)$ [HU]. Coronal and sagittal view reconstruction images' intensity range is $(-160, 240)$ [HU].

vantageous compared to the other algorithms such as BM3D or MBIR TV. Proposed method takes approximately 1.6 seconds

per slice for reconstruction which have 512×512 pixels with MATLAB implementation using a dual graphical processing

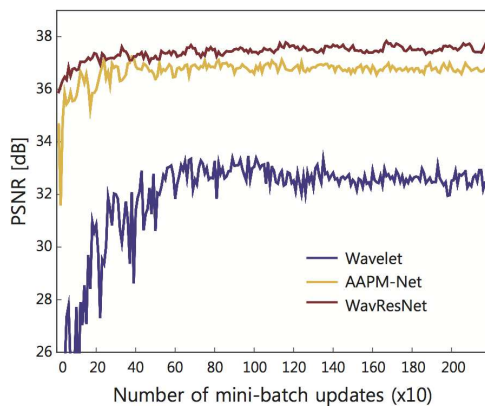


Fig. 8. Convergence plots of PSNR [dB] with respect to each mini-batch updates.

unit (NVidia GeForce Titan).

V. CONCLUSION

In this paper, we proposed a wavelet domain residual network (WavResNet) for low-dose X-ray CT reconstruction. To provide the theoretical background for performance improvement, we employed the recent proposal of deep convolutional framelets that interprets a deep learning as a multilayer implementation of convolutional framelets with ReLU nonlinearity. By combining the redundant global transform, residual network and signal boosting from concatenation layers, WavResNet provided significant improvement compared to the prior work by retaining the detailed texture. Using extensive experimental results, we showed that WavResNet is good at streaking noise reduction and preserving the texture details of the organs while the lesion information is maintained.

VI. ACKNOWLEDGEMENT

The authors would like to thanks Dr. Cynthia MaCollough, the Mayo Clinic, the American Association of Physicists in Medicine (AAPM), and grant EB01705 and EB01785 from the National Institute of Biomedical Imaging and Bioengineering for providing the Low-Dose CT Grand Challenge data set. This work is supported by Korea Science and Engineering Foundation, Grant number NRF-2016R1A2B3008104.

REFERENCES

- [1] J. Hsieh, *Computed tomography: principles, design, artifacts, and recent advances*. SPIE press, 2003, vol. 114.
- [2] M. Beister, D. Kolditz, and W. A. Kalender, "Iterative reconstruction methods in x-ray CT," *Physica medica*, vol. 28, no. 2, pp. 94–108, 2012.
- [3] S. Ramani and J. A. Fessler, "A splitting-based iterative algorithm for accelerated statistical x-ray CT reconstruction," *IEEE transactions on medical imaging*, vol. 31, no. 3, pp. 677–688, 2012.
- [4] E. Y. Sidky and X. Pan, "Image reconstruction in circular cone-beam computed tomography by constrained, total-variation minimization," *Physics in medicine and biology*, vol. 53, no. 17, p. 4777, 2008.
- [5] A. Krizhevsky, I. Sutskever, and G. E. Hinton, "Imagenet classification with deep convolutional neural networks," in *Advances in neural information processing systems*, 2012, pp. 1097–1105.
- [6] H. C. Burger, C. J. Schuler, and S. Harmeling, "Image denoising: Can plain neural networks compete with BM3D?" in *2012 IEEE Conference on Computer Vision and Pattern Recognition (CVPR)*. IEEE, 2012, pp. 2392–2399.

- [7] X. Mao, C. Shen, and Y.-B. Yang, "Image restoration using very deep convolutional encoder-decoder networks with symmetric skip connections," in *Advances in Neural Information Processing Systems*, 2016, pp. 2802–2810.
- [8] K. Zhang, W. Zuo, Y. Chen, D. Meng, and L. Zhang, "Beyond a gaussian denoiser: Residual learning of deep CNN for image denoising," *arXiv preprint arXiv:1608.03981*, 2016.
- [9] O. Ronneberger, P. Fischer, and T. Brox, "U-net: Convolutional networks for biomedical image segmentation," in *International Conference on Medical Image Computing and Computer-Assisted Intervention*. Springer, 2015, pp. 234–241.
- [10] J. Kim, J. Kwon Lee, and K. Mu Lee, "Accurate image super-resolution using very deep convolutional networks," in *Proceedings of the IEEE Conference on Computer Vision and Pattern Recognition*, 2016, pp. 1646–1654.
- [11] E. Kang, J. Min, and J. C. Ye, "A deep convolutional neural network using directional wavelets for low-dose x-ray CT reconstruction," *arXiv preprint arXiv:1610.09736 (to appear in Medical Physics)*, 2016.
- [12] H. Chen, Y. Zhang, M. K. Kalra, F. Lin, P. Liao, J. Zhou, and G. Wang, "Low-dose CT with a residual encoder-decoder convolutional neural network (RED-CNN)," *arXiv preprint arXiv:1702.00288*, 2017.
- [13] J. C. Ye and Y. S. Han, "Deep convolutional framelets: A general deep learning for inverse problems," *arXiv preprint arXiv:1707.00372*, 2017.
- [14] R. Yin, T. Gao, Y. M. Lu, and I. Daubechies, "A tale of two bases: Local-nonlocal regularization on image patches with convolution framelets," *SIAM Journal on Imaging Sciences*, vol. 10, no. 2, pp. 711–750, 2017.
- [15] J. C. Ye, J. M. Kim, K. H. Jin, and K. Lee, "Compressive sampling using annihilating filter-based low-rank interpolation," *IEEE Transactions on Information Theory*, vol. 63, no. 2, pp. 777–801, Feb. 2017.
- [16] K. H. Jin and J. C. Ye, "Annihilating filter-based low-rank Hankel matrix approach for image inpainting," *IEEE Transactions on Image Processing*, vol. 24, no. 11, pp. 3498–3511, 2015.
- [17] K. H. Jin, D. Lee, and J. C. Ye, "A general framework for compressed sensing and parallel MRI using annihilating filter based low-rank hankel matrix," *IEEE Trans. on Computational Imaging*, vol. 2, no. 4, pp. 480–495, Dec 2016.
- [18] G. Ongie and M. Jacob, "Off-the-grid recovery of piecewise constant images from few fourier samples," *SIAM Journal on Imaging Sciences*, vol. 9, no. 3, pp. 1004–1041, 2016.
- [19] D. Lee, K. H. Jin, E. Y. Kim, S.-H. Park, and J. C. Ye, "Acceleration of MR parameter mapping using annihilating filter-based low rank hankel matrix (ALOHA)," *Magnetic resonance in medicine*, vol. 76, no. 6, pp. 1848–1868, December 2016.
- [20] J. Lee, K. H. Jin, and J. C. Ye, "Reference-free single-pass EPI Nyquist ghost correction using annihilating filter-based low rank Hankel matrix (ALOHA)," *Magnetic resonance in medicine*, vol. 76, no. 8, pp. 1775–1789, December 2016.
- [21] K. H. Jin, J.-Y. Um, D. Lee, J. Lee, S.-H. Park, and J. C. Ye, "Mri artifact correction using sparse+ low-rank decomposition of annihilating filter-based hankel matrix," *Magnetic resonance in medicine*, vol. 78, no. 1, pp. 327–340, 2017.
- [22] J. Zhou, A. L. Cunha, and M. N. Do, "Nonsubsampled contourlet transform: construction and application in enhancement," in *IEEE International Conference on Image Processing 2005*, vol. 1. IEEE, 2005, pp. I–469.
- [23] A. Vedaldi and K. Lenc, "Matconvnet: Convolutional neural networks for Matlab," in *Proceedings of the 23rd ACM international conference on Multimedia*. ACM, 2015, pp. 689–692.
- [24] T. Flohr, K. Stierstorfer, S. Ulzheimer, H. Bruder, A. Primak, and C. H. McCollough, "Image reconstruction and image quality evaluation for a 64-slice CT scanner with z-flying focal spot," *Medical physics*, vol. 32, no. 8, pp. 2536–2547, 2005.
- [25] F. Noo, M. DeFrise, and R. Clackdoyle, "Single-slice rebinning method for helical cone-beam CT," *Physics in medicine and biology*, vol. 44, no. 2, p. 561, 1999.
- [26] Z. Wang, A. C. Bovik, H. R. Sheikh, and E. P. Simoncelli, "Image quality assessment: from error visibility to structural similarity," *IEEE transactions on image processing*, vol. 13, no. 4, pp. 600–612, 2004.
- [27] K. Dabov, A. Foi, V. Katkovnik, and K. Egiazarian, "Image denoising by sparse 3-d transform-domain collaborative filtering," *IEEE Transactions on image processing*, vol. 16, no. 8, pp. 2080–2095, 2007.
- [28] A. Chambolle, "An algorithm for total variation minimization and applications," *Journal of Mathematical imaging and vision*, vol. 20, no. 1, pp. 89–97, 2004.